encit 2020

ABCM Associação Brasileira de Engenharia e Ciências Mecânicas

18th Brazilian Congress of Thermal Sciences and Engineering
November 16-20, 2020, Online, RS, Brazil

ENC-2020-0658
THERMAL PERFORMANCE OF THE EXOTHERMIC REACTION OF THE PARTIAL OXIDATION OF METHANE IN A FLUIDIZED BED REFORMER: MATHEMATICAL MODELLING AND COMPUTER SIMULATION

Daniel Ribeiro Dessaune
Vitória da Fonseca Dias
Jornandes Dias da Silva
Polytechnic School - UPE, Laboratory of Environmental and Energetic Technology; Rua Benfica - 455, Madalena, Recife - PE, Brazil, Cep: 50750-470
daniel.dessaune@gmail.com
vi.dias11@hotmail.com
jornandesdias@poli.br

Abstract. *TFB reformers have been substantially studied in the past years as a promising reformer to study the thermochemical conversion of methane (CH_4). A variety of researches has been approached in the experimental field and theoretical. This work has as main objective a theoretical modelling to describe the process variables of The Catalytic Partial Oxidation of Methane (CPOM) on the TFB reformer. These process variables describe the specific aims as from each equation of the physical-mathematical model characterizing the performance from reactor. When the CH_4/O_2 ratio decreases on the CPOM method in TFB reformer, the reaction temperature is notably increased. A rise of the $u_{g,avg}$ indicates a decrease on the reaction temperature profiles in TFB reformer and thus, a reduction in the heat release by the CPOM method. An increase of the operating temperature has a significant role of the TC of CH_4 because of the higher consumption of reactants from CPOM's reactions.*

Keywords: *Solid open-cell foams, fluidized bed, TFB reformer, CPOM method, physical-mathematical model*

1. INTRODUCTION

The Catalytic Partial Oxidation of Methane (CPOM) is currently considered a promising process for so-called synthesis gas (H_2 and CO). The synthesis gas (syngas) can be obtained from various fuels among which natural gas is of special importance. The CPOM can be processed on the porous materials bed as solid open-cell foams due to high porosity and great surface area. Solid open-cell foams are macroporous reticulated 3D structures constituted by interconnected cavities and made of metals (aluminum, steel), ceramics (alumina, silicon carbide etc.), or carbon materials. In the field of the catalyst reforming process, solid open-cell foams have been tested for the steam reforming of methane and dry reforming of Methane (Chen et al., 2018; Wang et al., 2015). These researchers had reported results of reforming processes using fixed bed reformers, but these authors didn't provide orientation when these reformers were used to process the CPOM on the solid open-cell foam bed. We fill this gap with the approaches indicated by these authors and extend a novel approach for the CPOM process using a Thermochemical Fluidized Bed (TFB) reformer. Recently, TFB reformers have been considerably attracted the interest of many researchers because of their ability to obtain syngas with high energetic density (Lima et al., 2020; Nourbakhsh et al., 2019).

The CPOM's combustion reaction is strongly exothermal and it can be used to convert methane (CH_4) into hydrogen (H_2). The CPOM's method includes the thermochemical conversion of CH_4 after occurring chemical dissociation process (Yazdia et al., 2020). As negative effect of the CPOM process, due to the highly exothermic nature of the CPOM reaction, hot-spots with serious consequences are formed in the TFB reformers. On the other hand, it should be mentioned that injecting an inert diluting gas such as nitrogen (N_2) to overcome the challenge of hot-spot formation will itself increase the process unit's costs. Having considered the challenges of the CPOM method, it is also acceptable to look at its potentials for being integrated with other processes (Wu et al., 2020). For example, significant portion of the released heat in reforming reactor can be explored in an endothermic reforming of CH_4.

The mathematical modelling is important to design and optimize the reformer types in order to understand its behavior for a given reaction system. Full mathematical models can be developed from transport equations of chemical components, energy and momentum swing equations for the gas phase as well as transport equations of chemical components, energy and momentum balance equations to the solid phase (Cruz and Silva, 2017). Herein, developed

mathematical modelling of the TFB reformer consists of a detailed model that involves the energy balances and transport equations of chemical components on the catalytic bed. A Non-Isothermal Pseudo-Homogeneous Mathematical (NIPHM) model is used to model the CPOM method in TFB reformer.

With the purpose to reduce the research cost and project time, the mathematical modelling and computer simulation are extensively used to obtain a better understanding of design parameters in reformers. The development and solution of the physical-mathematical models are still a novelty of TFB reformers to obtain the sustainable clean energy and thus the topic is a very actual in open literature. The novelty of the present work lies in the use of open-cell foam (Al_2O_3) bed for the CPOM method. The effects of the CH_4/O_2 ratio and $u_{g,avg.}$ on the reaction Temperature are numerically investigated in TFB reformer. In addition, the operating temperature's effect on the TC of CH_4 will be verified for the CPOM method from TFB reformer.

2. PHYSICAL SETUP

A schematic setup is used to study the thermochemical conversion of the CPOM method in TFB reformer according to Fig. 1. The physical model from TFB reformer is shown in Fig. 1.

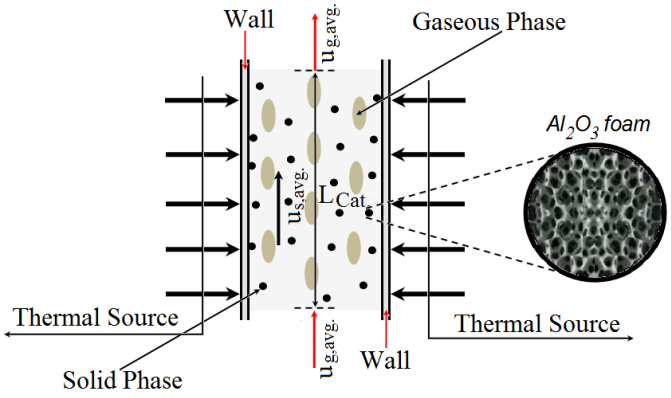

Figure 1. Schematic setup of the physical model from TFB reformer to study the CPOM method.

2.1 Thermochemical kinetic model

The CPOM method's main reactions on the catalyst bed contain two reactions including the combustion of CH_4 and SRM (Silva and Abreu, 2016; Ji et al., 2003). However, major reactions involved in CPOM method are reported as follows:

$$CPOM: CH_{4(g)} + O_{2(g)} \rightarrow CO_{2(g)} + 2H_2O_{(g)}\,;\ \Delta H^0_{298K} = -802.0\,kJ/mol \tag{1a}$$

$$SRM: CH_{4(g)} + H_2O_{(g)} \rightleftarrows CO_{(g)} + 3H_{2(g)}\,;\ \Delta H^0_{298K} = +206.1\,kJ/mol \tag{1b}$$

The above reaction (1a) is highly exothermic. On the other hand, the above reaction (1b) is highly endothermic. The overall rate equations of reactions, Eq. (1a) and (1b), are based on the Langmuir-Hinshelwood kinetic model. Therefore, its global kinetic rates are reported as follows.

$$R_{CPOM} = \frac{k_{1,CPOM}\, x_{CH_4}\, x_{O_2}}{\left(1 + K_{CH_4,0}\, x_{CH_4} + K_{O_2,0}\, x_{O_2}\right)^2} + \frac{k_{2,CPOM}\, x_{CH_4}\, x_{O_2}^{1/2}}{\left(1 + K_{CH_4,0}\, x_{CH_4} + K_{O_2,0}\, x_{O_2}\right)} \tag{2a}$$

$$R_{SRM} = \frac{\frac{k_{SRM}}{P_{H_2}^{2.5}}\left(P_{CH_4}\, P_{H_2O} - \frac{P_{H_2}^3\, P_{CO}}{K_{SRM}}\right)}{\left(1 + \frac{F_{H_2O,0}}{F_{CH_4,0}} + \frac{F_{H_2,0}}{F_{CH_4,0}} + K_{CO}P_{CO} + K_{H_2}P_{H_2} + K_{CH_4}P_{CH_4} + \frac{K_{H_2O}P_{H_2O}}{P_{H_2}}\right)^2} \tag{2b}$$

The partial pressures of chemical components i, i = CH_4, H_2O, CO, and H_2, from Eq. (1b) are computed using Eqs. (2c) and (2d) as follows.

$$P_{CH_4} = \frac{1-\left(1-\frac{F_{CH_4}}{F_{CH_4}\rho}\right)}{1+\sum_j^3 \frac{F_j\rho}{F_{CH_4}\rho}} P_{op.};\ P_{H_2O} = \frac{\frac{F_{H_2O}\rho}{F_{CH_4}\rho}-\left(1-\frac{F_{CH_4}}{F_{CH_4}\rho}\right)-\left(\frac{F_{CO_2}}{F_{CH_4}\rho}\right)}{1+\sum_j^3 \frac{F_j\rho}{F_{CH_4}\rho}} P_{op.};\ j = H_2O, CO,\ and\ H_2 \tag{2c}$$

$$P_{CO} = \frac{\frac{F_{CO}\rho}{F_{CH_4}\rho}+\left(1-\frac{F_{CH_4}}{F_{CH_4}\rho}\right)-\left(\frac{F_{CO_2}}{F_{CH_4}\rho}\right)}{+\sum_j^3 \frac{F_j\rho}{F_{CH_4}\rho}} P_{op.};\ P_{H_2} = \frac{\frac{F_{H_2}\rho}{F_{CH_4}\rho}+3\left(1-\frac{F_{CH_4}}{F_{CH_4}\rho}\right)-\left(\frac{F_{CO_2}}{F_{CH_4}\rho}\right)-\frac{F_{H_2}}{F_{CH_4}\rho}}{+\sum_j^3 \frac{F_j\rho}{F_{CH_4}\rho}} P_{op.} \tag{2d}$$

The net rates (r_i) for each chemical component i (i = CH_4, H_2O, CO, and H_2) are computed using Eq. (2e) and therefore, these rates are considered in transport equations of chemical components (Cruz and Silva, 2017).

$$r_i = \sum_{i=1}^4 \sum_{j=1}^2 \eta_j\, \sigma_{ij} R_j \tag{2e}$$

The kinetic constants, equilibrium constants and adsorption equilibrium constants for the calculations of reaction rates are described as a function of operating temperature (Cruz and Silva, 2017).

$$k_{SRM} = 2.636\, x\, 10^{13}\, exp\left(-\frac{240.10}{R_u\, T_{op.}}\right), \left(mal\,(kPa)^{0.5} / kg_{cat.}\, sec.\right) \tag{3a}$$

$$K_{SEM} = 1.0267 x 10^4\, exp\left(-\frac{26830.0}{T_{op.}}\right) + 30.114\,, \left(kPa^2\right) \tag{3b}$$

$$K_{CH_4} = 6.650 x 10^{-6}\, exp\left(-\frac{38.28}{R_u T_{op.}}\right), \left(kPa^{-1}\right) \tag{3c}$$

$$K_{H_2} = 6.120 x 10^{-11}\, exp\left(\frac{82.90}{R_u T_{op.}}\right), \left(kPa^{-1}\right) \tag{3d}$$

$$K_{CO} = 8.230 x 10^{-7}\, exp\left(\frac{70.65}{R_u T_{op.}}\right), \left(kPa^{-1}\right) \tag{3e}$$

$$K_{H_2O} = 1.770 x 10^5\, exp\left(-\frac{88.68}{R_u T_{op.}}\right), (-) \tag{3f}$$

2.2 Mathematical modelling

A thermochemical modelling is used to model the CPOM method in TFB reformer. Thus, a NIPHM model is built to study the thermochemical performance inside TFB reformer. This NIPHM model had been constructed by a system of Nonlinear Partial Differential Equations (NPDEs) that couples to a complex kinetic model of the CPOM reaction. The development of the NIPHM model takes into account the following assumptions: (1) the NIPHM model from TFB reformer is plug-flow with axial dispersion under transient condition, (2) the radial dispersion is negligible inside TFB reformer, (3) the gaseous mixture has constant density in TFB reformer, (4) the deposition effect of carbon at the surface of catalytic particles has been neglected, (5) the gas behavior inside TFB reformer was considered as an ideal gas mixture, (6) the bed porosity in axial direction is considered constant, and (7) chemical reaction is assumed to take place at the surface of catalyst particles. These premises are developed to construct the governing equations of the NIPHD model inside TFB reformer as follows.

2.3 Gas phase's energy balance

A dynamic equation is developed to describe the heat distribution on the gas phase inside TFB reformer. The developed equation provides clear information to drive the temperature distribution on the gas phase in porous medium of the catalyst bed. Thus, an one-dimensional dynamic equation is developed for the gas phase's temperature as follows.

$$\rho_{g,mix.} C_{p,g,mix.} \left(\frac{\partial T_g}{\partial t} + u_{g,avg.} \frac{\partial T_g}{\partial z} \right) = \lambda_{g,eff} \frac{\partial^2 T_g}{\partial z^2} - h_{gs} \frac{\left(1-\varepsilon_b\right)}{\varepsilon_b} \frac{6}{d_p} \left(T_g - T_r \right) \tag{4a}$$

The effective thermal conductivity of the gas phase is defined as a function of the gas thermal conductivity as follows.

$$\lambda_{g,eff.} = \varepsilon_b \, \lambda_{g,mix.}; \; \lambda_{g,mix.} = 1.52x10^{-11} T_{g,0}^3 - 4.86x10^{-8} T_{g,0}^2 + 1.02x10^{-4} T_{g,0} - 3.93x10^{-3} \tag{4b}$$

The suitable initial and boundary conditions from Eq. (4a) are given as follows.

$$T_g\Big|_{t=0} = T_{g,0}; \; 0 \le z \le L \tag{4c}$$

$$\left.\frac{\partial T_g}{\partial z}\right|_{z=0^+} = \frac{\rho_{g,mix.} C_{p,g,mix.} u_{g,avg.}}{\lambda_{g,mix.}} \left(T_g\Big|_{z=0^+} - T_{g,\infty} \right); \; t \ge 0 \tag{4d}$$

$$\left.\frac{\partial T_g}{\partial z}\right|_{z=L} = \frac{h_{gs,eff.}}{\lambda_{g,eff.}} \left(T_{g,\infty} - T_g\Big|_{z=L} \right); \; t \ge 0 \tag{4e}$$

2.4 Solid phase's energy balance

The energy balance is constructed at the surface of solid particles where takes place the exothermic reaction of CH_4. The model equation includes the solid phase's convection effect, effective thermal dispersion, the gas-solid heat transfer, and global rate of CPOM reaction. As result, the governing equation for the solid phase is defined as follows.

$$\rho_s C_{p,s} \left(\frac{\partial T_r}{\partial t} + u_{s,avg.} \frac{\partial T_r}{\partial z} \right) = \lambda_{s,eff} \frac{\partial^2 T_r}{\partial z^2} + h_{sg} \frac{6}{d_p} \frac{\left(1-\varepsilon_b\right)}{\varepsilon_b} \left(T_g - T_r \right) + \rho_s \frac{\left(1-\varepsilon_p\right)}{\varepsilon_p} \Big[\left(-\Delta H_{CPOM} \right) \eta_{CPOM} R_{CPOM} + \left(+\Delta H_{SRM} \right) \eta_{SRM} R_{SRM} \Big]; \; 0 \le z \le L, t > 0 \tag{5a}$$

The thermal conductivity of the solid phase is defined as a function of the thermal conductivity from the gaseous mixture according to Eq. (5a) below.

$$\lambda_{s,eff} = \left(1-\varepsilon_b\right) \lambda_{g,mix.} \tag{5b}$$

The initial and boundary conditions from Eq. (5a) are described as:

$$T_r\Big|_{t=0} = T_{r,0}; \; 0 \le z \le L \tag{5c}$$

$$-\left.\frac{\partial T_r}{\partial z}\right|_{z=0^+} = \frac{\rho_s C_{p,s} u_{s,avg.}}{\lambda_s} \left(T_r\Big|_{z=0^+} - T_{r,\infty} \right); \; t \ge 0 \tag{5d}$$

$$\left.\frac{\partial T_r}{\partial z}\right|_{z=L} = \frac{h_{sg,eff}}{\lambda_{s,eff.}} \left(T_{r,\infty} - T_r\Big|_{z=L} \right); \; t \ge 0 \tag{5e}$$

2.5 Transport equation of chemical components

Based on assumptions mentioned in section 2.2, chemical components of the CPOM method in TFB reformer are modelled by Eq. (6a). Eq. (6a) reports the transport equations for chemical components i (i = CH_4, H_2O, O_2, CO, CO and H_2) as follows.

$$\frac{u_{g,avg.}}{g}\frac{\partial F_i}{\partial t}+\frac{u_{g,avg.}}{S_{sp}}\frac{\partial F_i}{\partial z}=\frac{D_{ax,i}}{S_{sp}}\frac{\partial^2 F_i}{\partial z^2}+\rho_s\, r_{ref.}^2\, L\left(1-\varepsilon_b\right)r_i\,;\,0<z<L \tag{6a}$$

The suitable initial and boundary conditions from Eq. (6a) are presented as follows.

$$F_i\Big|_{t=0}=F_{i,0};\,0\le z\le L \tag{6b}$$

$$\varepsilon_b\frac{D_{ax,i}}{L}\frac{\partial F_i}{\partial z}\bigg|_{z=0^+}=u_{g,avg.}\left(F_i\Big|_{z=0^+}-F_{i,\infty}\right);\,t\ge 0 \tag{6c}$$

$$\varepsilon_b\frac{D_{ax,i}}{L}\frac{\partial F_i}{\partial z}\bigg|_{z=L}=k_{gs,eff}\left(F_i\Big|_{z=L}-F_{i,\infty}\right);\,t\ge 0 \tag{6d}$$

2.6 Numerical solution of the model equation

Because of the numerical stability, the literature has been presented several numerical methods to solve NPDEs. The selection of the numeric method is dependent on the desired accuracy, numeral stability, and robustness of results while maintaining computational efficiency. The numerical solution of the NIPHM model has been driven for a numeric method which ensures the numerical stability (Silva and Abreu, 2016). Therefore, the developed model was solved by the finite volume method (FVM) in together with prescribed initial and boundary conditions to analyze the performance of the CPOM method in TFB reformer.

3. RESULTS AND DISCUSSIONS

In section 2, a physical-mathematical modelling has been developed to investigate the CPOM method in TFB reformer. This physical-mathematical model was built to study the thermochemical performance of the CPOM method using an additional thermal source. A computational algorithm using the FORTRAN 95 has been elaborated by authors to compute the CPOM method's variables in TFB reformer.

3.1 Kinetic parameters

In Section 2.1, kinetic model's equations were presented. The kinetic model's parameters are used to feed the computational algorithm in combination with hydrodynamic model's parameters from TFB reformer. The numerical values of the kinetic model's parameters are reported in Table 1 below.

Table 1. Kinetic parameters, equilibrium constants of reactions and equilibrium constants

Parameters kinetic, equilibrium, and adsorption	Values	Sources
$k_{1,\,CPOM}$ (mol/$kg_{cat.}$ sec.)	3.14×10^{-4}	Ji et al., 2003
$K_{2,\,CPOM}$ (mol/$kg_{cat.}$ sec.)	2.64×10^{-4}	Ji et al., 2003
$K_{CH4,\,0}$ (-)	6.67×10^{-2}	Ji et al., 2003
$K_{O2,\,0}$ (-)	4.34×10^{-5}	Ji et al., 2003
k_{SRM} [mol (kPa)$^{0.5}$/$kg_{cat.}$ sec.]$^{(1)}$	7.39×10^{13}	Eq. (3a)
$K_{eq.,\,1}$ (kPa^2)$^{(1)}$	2.13×10^{7}	Eq. (3b)
K_{CH4} (kPa^{-1})$^{(1)}$	9.87×10^{-7}	Eq. (3c)
K_{H2O} (-)$^{(1)}$	2.61×10^{4}	Eq. (3d)
K_{H2} (kPa^{-1})$^{(1)}$	5.48×10^{-12}	Eq. (3e)
K_{CO} (kPa^{-1})$^{(1)}$	7.43×10^{-6}	Eq. (3f)
$\eta_{CPOM}{}^{(1)}$ (-)	0.037	Cruz and Silva, 2017
$\eta_{SRM}{}^{(1)}$ (-)	0.015	Cruz and Silva, 2017
x_{O2}	0.032	Silva and Abreu, 2016
x_{CH4}	0.071	Silva and Abreu, 2016

(1) Computed at 700°C

3.2 Hydrodynamic parameters from TFB reformer

In Section 2.2, hydrodynamic model's equations have been described. Hydrodynamic model's parameters are used to feed the computational algorithm and these parameters are reported in Table 2 below.

Table 2. Model parameters and inlet operating conditions of the CPOM method in TFB reformer.

Model parameters	Values	Sources
L (m)	0.18	Estimated
d_p (m)	7.9×10^{-5}	Estimated
$d_{refor.}$ (m)	4.2×10^{-3}	Estimated
$T_{g,0}$ (K)	873	Estimated
$T_{r,0}$ (K)	873	Estimated
$P_{op.}$ (kPa)	500	Estimated
$\rho_{g,\,mix.}$ (kg/m^3)	0.1692	Silva and Abreu, 2016
$C_{p,\,g,\,mix.}$ (kJ/kg K)	121.67	Dias and Silva, 2020
$u_{g,\,mix}$ (m/sec.)	0.131	Dias and Silva, 2020
$\lambda_{g,\,eff.}$ (W/m K)	147.13	Eq. (4b)
H_{gs} (W/m^2 K)	0.037	Dias and Silva, 2020
ε_b (m^3 gas/m^3 reformer)	0.39	Dias and Silva, 2020
ρ_s (kg/m^3)	590	Voltolina et al., 2017
$C_{p,\,s.}$ (kJ/kg K)	1.214	Dias and Silva, 2020
$u_{s,\,mix}$ (m/sec.)	0.017	Dias and Silva, 2020
$\lambda_{s,\,eff.}$ (W/m K)	126.31	Eq. (5b)
ε_p (m^3 gas/m^3 reformer)	0.88	Voltolina et al., 2017
g (m/sec.)	3.53×10^4	Silva and Abreu, 2016
S_{sp} (sec.$^{-1}$)	2.21×10^{-4}	Silva and Abreu, 2016
$D_{ax,\,CH4}$ (m^2/sec.)	5.28×10^{-6}	Silva and Abreu, 2016
$D_{ax,\,O2}$ (m^2/sec.)	4.97×10^{-5}	Silva and Abreu, 2016
$D_{ax,\,H2O}$ (m^2/sec.)	2.98×10^{-6}	Silva and Abreu, 2016
$D_{ax,\,H2}$ (m^2/sec.)	1.21×10^{-6}	Silva and Abreu, 2016
$D_{ax,\,CO}$ (m^2/sec.)	3.17×10^{-6}	Silva and Abreu, 2016
$D_{ax,\,CO2}$ (m^2/sec.)	9.87×10^{-6}	Silva and Abreu, 2016

3.3 Numerical experiments of the reaction temperature

Fig. 2 shows that the range of the CH_4/O_2 ratio, at the inlet from TFB reformer, has a pertinent effect on the reaction profile inside TFB reformer itself. Different values of the CH_4/O_2 ratio were used to check the effect of this ratio on the reaction temperature.

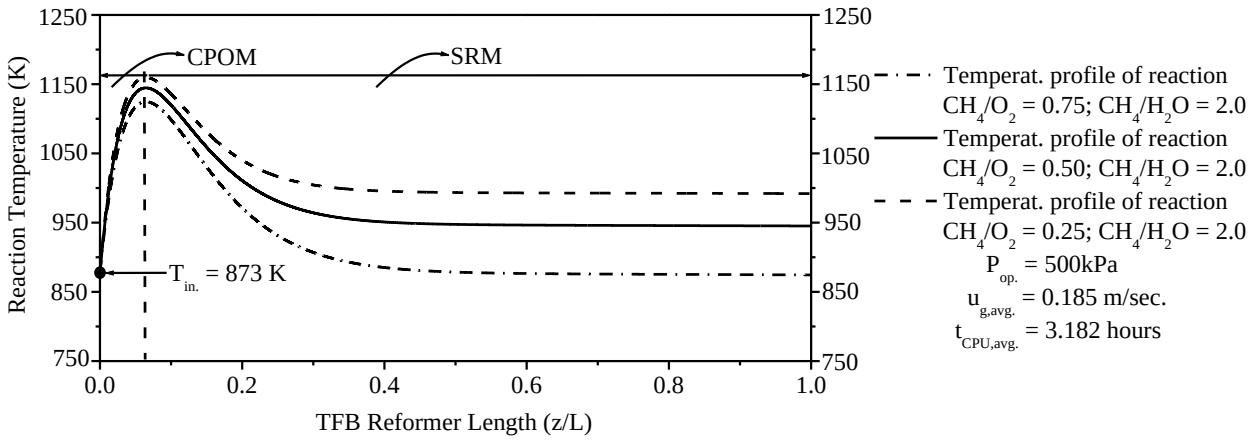

Figure 2. Profiles of the reaction temperature along of the TFB reformer length at different molar ratios of CH_4/O_2.

It was reported that Reaction Temperature Profiles (RTPs) tend to assume an inflection point of maximum values in which the effective temperature of the CPOM method is optimal. The location (± 0.46) of maximum values could be owing to the interaction of many factors like the composition of the catalyst bed, initial temperature, operating pressure,

and the thermodynamic equilibrium of endothermic reaction. As results, when molar ratio (CH_4/O_2 = 0.25) at the TFB reformer's inlet is low, the released heat of the CPOM reaction (Eq. (1a)) has notably effect on the RTP and thus, the RTP is increased. On the other hand, when molar ratio (CH_4/O_2 = 0.75) at the TFB reformer's inlet is higher, the released heat of the CPOM reaction (Eq. (1a)) has remarkably effect on the RTP and therefore, the RTP is reduced. It is clearly shown that the ERP reaches the stable state at about ± z/L = 0.4 from TFB reformer length. After reaching the stable state, the RTPs are maintained constant up to z/L = 1.0 from TFB reformer with values of 875.46 K (CH_4/O_2 = 0.75), 947.21 K (CH_4/O_2 = 0.5), and 998.57 K (CH_4/O_2 = 0.25), respectively.

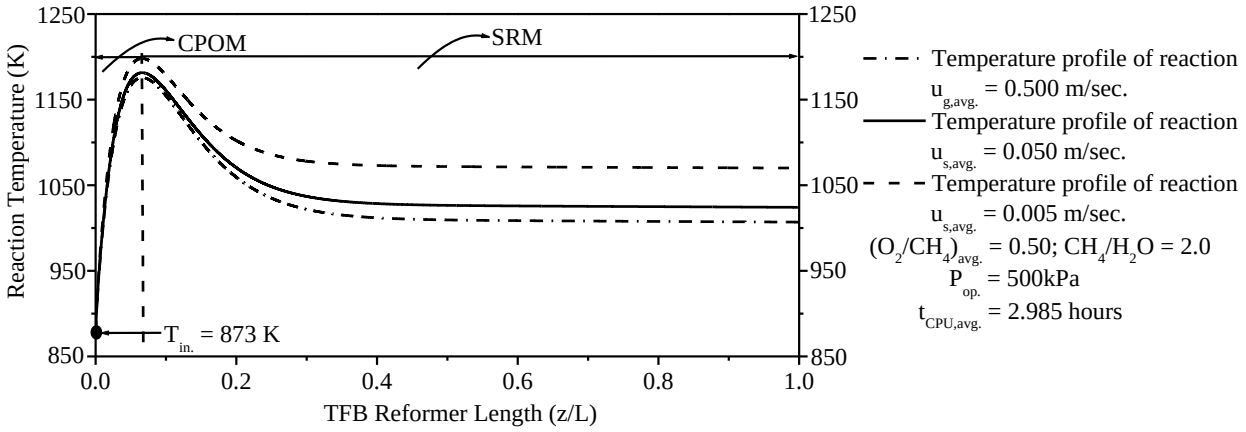

Figure 3. Profiles of the reaction temperature along of the TFB reformer length at different average gas velocities.

After investigating the effect of the molar ratio of CH_4/O_2 on the RTPs from TFB reformer, authors have also studied the effect of the average gas superficial velocity ($u_{g,avg}$) on these profiles. As seen Fig. 2, an inflection point is also verified in Fig. 3. The location is reported on the RTPs at about ± 0.31. As results, an increase of the $u_{g,avg}$ indicates a decrease on the RTPs in TFB reformer and therefore, a reduction of the heat rate on the CPOM method. Unlike, a decrease of the $u_{g,avg}$ points an increase on the RTPs in TFB reformer and thus, a rise of the heat rate on the CPOM method. In fact, Fig. 3 shows the effect of the $u_{g,avg}$ on the RTPs inside TFB reformer. As it was analyzed in Fig. 2, three different values of the $u_{g,avg}$ were used to check the sensibility of the RTP to $u_{g,avg}$. Fig. 3 reports that when the $u_{g,avg}$ is lower ($u_{g,avg}$ = 0.005 m/sec.), the RTP is notably increased. Opposing, when the $u_{g,avg}$ is higher ($u_{g,avg}$ = 0.500 m/sec.), the RTP is remarkably reduced. After achieving the stable state (z/L = ± 0.40), RTP s are kept constant up to z/L = 1.0 on TFB reformer with values at about 1005.34 K ($u_{g,avg}$ = 0.5 m/sec.), 1027.18 K ($u_{g,avg}$ = 0.05 m/sec), and 1070.43 K ($u_{g,avg}$ = 0.005 m/sec.), respectively.

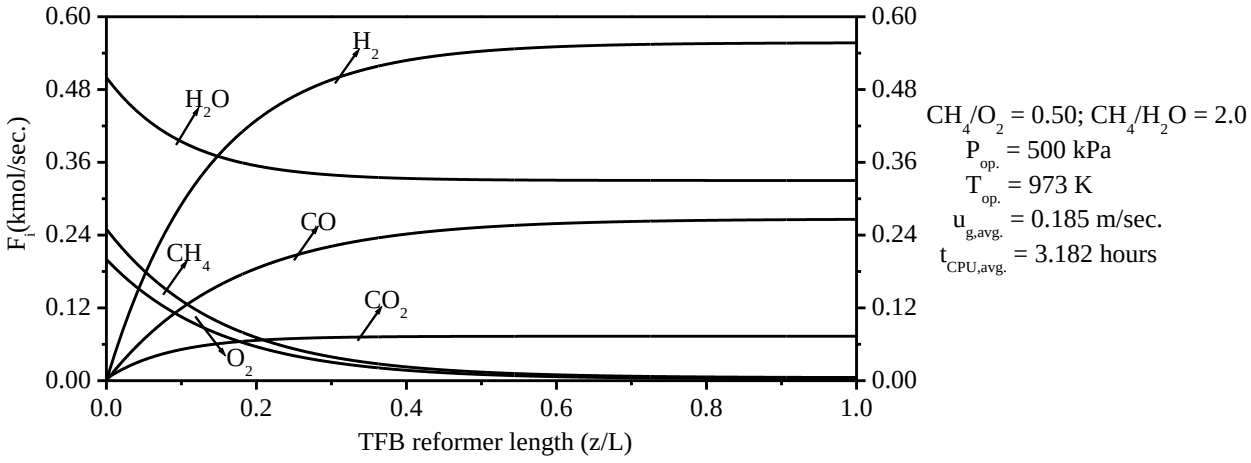

Figure 4. Molar flow profiles of components i along of the TFB reformer length.

Fig. 4 investigates the profiles of mole flows for each component i of the CPOM method TFB reformer at the following operating conditions: CH_4/O_2 = 0.5, H_2O/CH_4 = 2.0, 500 kPa, 973 K, and 0.185 m/sec. In this figure, the mole flow's profiles of the reactants (CH4, O_2, and H_2O) and products (CO, CO_2 and H_2) have been reported for the CPOM method from TFB reformer. H_2O was consumed by the CPOM method in only 42.37% of the TFB reformer length,

after that a stable state is reached up to z/L = 1.0. On the other hand, CH4 and O2 were consumed by the CPOM method in only 78.93% of the TFB reformer length, after that stable states are achieved until z/L = 1.0. After reaching 58.32% of the TFB reformer length, H_2 and CO achieve stable states with values of 55.71% and 26.59% at z/L = 1.0. On the other hand, After reaching 29.89% of the TFB reformer length, CO_2 arrives a stable state with value of 7.33% at z/L = 1.0.

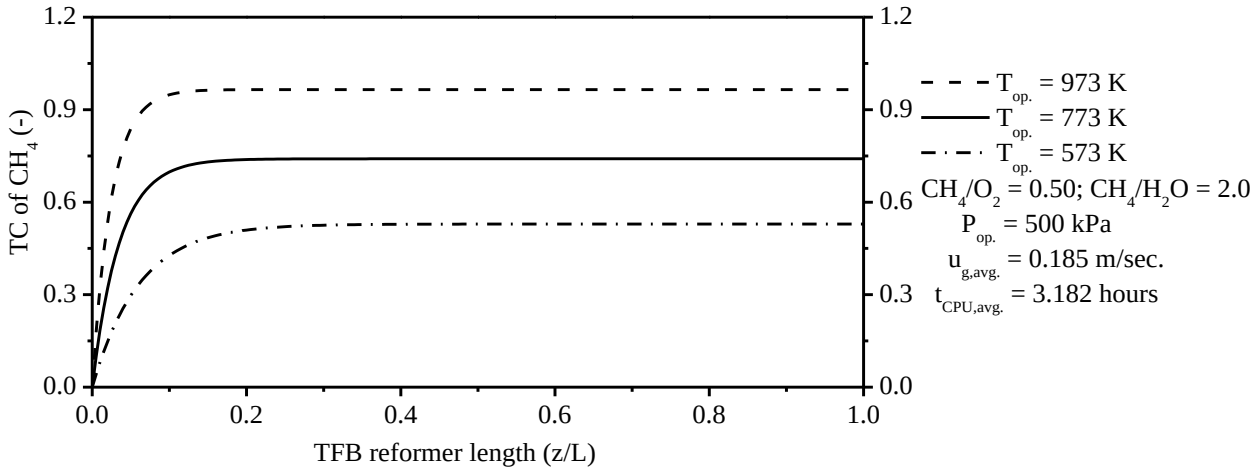

Figure 5. Effect of the operating temperature on the conversion of CH_4 along of the TFB reformer length.

Thermodynamic limitations of Packed Bed Reformers (PBRs) are considered as a great problem to increase the thermochemical conversion of the CPOM method. To solve this gap, it was used the TFB reformer as an innovating use that improves thermodynamic limitations and can perfect the thermochemical conversion. The thermochemical performance of TFB reformers can be analyzed from thermochemical conversion of CH_4 as follows

$$Thermochemical\,Conversion\left(TC\right)\,of\;\;CH_4 = 1 - \frac{F_{CH_4,out}}{F_{CH_4,0}} \tag{6a}$$

Fig. 5 shows the TC of CH_4 of the CPOM method in TFB reformer. It is clearly shown that the TC of CH4 is increasing with the operating temperature's rise. As results, after achieving the stable state (see Fig. (5)), the TC of CH_4 is kept constant up to z/L = 1.0 from TFB reformer with values of 52.67% (573 K), 74.06% (773 K), and 96.53% (973 K), respectively.

4. CONCLUSIONS

The present work has been focused towards a numerical analysis of the mathematical modelling and computer simulation to describe the performance of a TFB reformer using as reference method to CPOM. The model equations that describe the gas temperature, reactions temperature, molar flow of components i have been reported and discussed. The work's results highlighted the importance of the mathematical model developed to describe the performance from TFB reformer. In this context, main conclusions are summarized as follows.

1. The content of O_2 has an important effect on the reaction temperature, i.e., when the CH_4/O_2 is low, the reaction temperature is notably increased. Unlike, when the CH_4/O_2 ratio is higher, the reaction temperature is remarkably decreased.
2. The effect of the $u_{g,avg}$ has driven a significant role on the reaction temperature profiles. Similarly to the CH_4/O_2 ratio, when the $u_{g,avg}$ is low, the reaction temperature profiles are remarkably increased. Unlike, the reaction temperature profiles is reduced with the increase of the $u_{g,avg}$.
3. The effect of the operating temperature has driven a significant role the TC of CH_4. An increase of the operating temperature has a significant improvement of the TC of CH_4 due to the higher consumption of reactants from CPOM's reactions.

5. ACKNOWLEDGEMENTS

The authors of this paper would like to thank CNPq (National Council of Scientific and Technological Development) for the financial support given (Process 48354/2012).

6. LIST OF SYMBOLS

$C_{p, g, mix.}$ Molar heat capacity at constant pressure of the gas mixture (kJ/kg K)
$C_{p,s}$ Heat capacity pressure of the solid phase (kJ/kg K)
$D_{ax, i}$ Dispersion coefficients of each component i (m^2/sec.)
d_p Diameter of the solid particles (m)
F_i Molar flow of components i (kmol/sec.)
$F_{j,0}$ Initial molar flows of components j
g Gravity acceleration (m/sec.^{2})
h_{gs} Gas-solid heat transfer coefficient (W/m^2 K)
$k_{1,CPOM}$ Kinetic constant of the R_{CPOM} (kmol/$kg_{cat.}$ sec.)
$k_{2,CPOM}$ Kinetic constant of the R_{CPOM} (kmol/$kg_{cat.}$ sec.)
$K_{CH4,0}$ Adsorption constant of CH_4 in Eq. (2a) (-)
$K_{O2,0}$ Adsorption constant of O_2 in Eq. (2a) (-)
k_{SRM} Kinetic constant of the RSRM (Eq. (3a)) (kmol kPa^{-1}/$kg_{cat.}$ sec.)
K_{SRM} Equilibrium constant of the R_{SRM} (Eq. (3b)) (kPa^2)
K_i Adsorption constants of components i (Eqs. (3c)-(3e)), i = CO, H_2 and CH_4, (kPa^{-1})
K_j Adsorption constant of components j (Eq. (3f)), j = H_2O, (-)
L TFB reformer length (m)
P_i Partial pressures of components i (Eqs. (2c)-(2d)), i = CH_4, H_2O, CO, CO_2 and H_2, (kPa)
Pop. Operating pressure (kPa)
$r_{ref.}$ TFB reformer radius (m)
r_i Net rates of components i (i = CH_4, H_2O, CO, CO_2 and H_2) (kmol/$kg_{cat.}$ sec.)
R_j Overall rates of the reforming reactions j, j = 1 and 2, (kmol/$kg_{cat.}$ sec.)
S_{sp} Spatial velocity (sec^{-1})
t Iteration time (sec.)
$T_{er, 0}$ Initial temperature of the endothermic reaction (K)
T_{er} Temperature of the endothermic reaction (K)
$T_{g, 0}$ Gas phase's initial temperature (K)
T_g Gas phase's temperature (K)
$u_{g, avg.}$ Gas phase's average velocity (m/sec.)
$u_{s, avg.}$ Solid phase's average velocity (m/sec.)
z Axial coordinate (m)

7. GREEK LETTERS

ε_b Fluidized-bed porosity (m^3gas/m^3reformer)
ε_p Particle porosity (m^3particle/m^3reformer)
η_j Effectiveness factors of reforming reactions j (j = CPOM and SRM)
$\lambda_{g, mix.}$ Gaseous mixture's thermal conductivity (W/m K)
$\lambda_{g, eff.}$ Gas phase's effective thermal conductivity (W/m K)
$\lambda_{s, eff.}$ Solid phase's effective thermal conductivity (W/m K)
$\rho_{g, mix.}$ Gas mixture density of components i (kg/m^3)
ρ_s Solid phase density (kg/m^3)

8. REFERENCES

Balzarotti, R., Ambrosetti, M., Beretta, A., Groppi, G., Tronconi, E., 2020. “Investigation of packed conductive foams as a novel reactor configuration for methane steam reforming”. *Chemical Engineering Journal*, Vol. 391, pp. 123494.

Cruz, B. M., Silva, J. D., 2017. “A two-dimensional mathematical model for the catalytic steam reforming of methane in both conventional fixed-bed and fixed-bed membrane reformers for the production of hydrogen”. *International Journal of Hydrogen Energy*, Vol. 42, pp. 23670-23690.

Clark, R-J., Mehrabadi, A., Farid, M., 2020. "State of the art on salt hydrate thermochemical energy storage systems for use in building applications". *Journal of Energy Storage*, Vol. 27, pp. 101145.

Chen, X., Wang, F., Han, Y., Yu, R., Cheng, Z., 2018. “Thermochemical storage analysis of the dry reforming of methane in foam solar reactor”. *Energy Conversion and Management*, Vol. 158, pp. 489-498.

Dias, V. F., Silva, J. D., 2020. “Mathematical modelling of the solar - driven steam reforming of methanol for a solar thermochemical micro - fluidized bed reformer: thermal performance and thermochemical conversion”. *Braz. Soc. Mech. Sci Eng*., Vol. 42, pp. 447.

Dashliborun, A. M., Fatemi, S., Najafabadi, A. T., 2013. "Hydrogen production through partial oxidation of methane in a new reactor configuration". *International Journal of Hydrogen Energy*, Vol. 38, pp. 1901-1909.

Ji, P., Van der Kooi, H. J., de Swaan Arons, J., 2003. “Simulation and thermodynamic analysis of an integrated process with H_2 membrane CPO reactor for pure H_2 production”. *Chemical Engineering Science*, Vol. 58, pp. 3901-3911.

Lima, K. P. M., Dias, V. F. and Silva, J. D., 2020. “Numerical modelling for the solar driven bi-reforming of methane for the production of syngas in a solar thermochemical micro-packed bed reformer”. *International Journal of Hydrogen Energy*, Vol. 45, pp. 10353-10369.

Nourbakhsh, H., Shahrouzi, J. R., Ebrahimi, H., Zamaniyan, A., Nasr, M. R. J. “Experimental and numerical study of syngas production during premixed and ultra-rich partial oxidation of methane in a porous reactor”. *International Journal of Hydrogen Energy*, Vol. 44, pp. 31757-31771.

Silva, J. D. and Abreu, C. A. M., 2016. “Modelling and simulation in conventional fixed-bed and fixed-bed membrane reformers for the steam reforming of methane”. *International Journal of Hydrogen Energy*, Vol. 41, pp. 11669-11674.

Voltolina, S., Marín, P., Díz, F. V., Salvador, O., 2017. “Open-cell foams as beds in multiphase reactors: Residence time distribution and mass transfer”. *Chemical Engineering Journal*, Vol. 316, pp. 323 – 331.

Yazdia, M. R. M., Ommia, F., Ehyaeic, M. A., Rosend, M. A., 2020. "Comparison of gas turbine inlet air cooling systems for several climates in Iran using energy, exergy, economic, and environmental (4E) analyses". *Energy Conversion of Management*, Vol. 216, pp. 112944.

Wu, S., Zhou, C., Doroodchi, E., Moghtaderi., 2020. “Techno-economic analysis of an integrated liquid air and thermochemical energy storage system”. *Energy Conversion of Management*, Vol. 205, pp. 112341.

9. RESPONSIBILITY NOTICE

The author(s) is (are) the only responsible for the printed material included in this paper.